Journal of Materials Chemistry B

Accepted Manuscript

ROYAL SOCIETY OF CHEMISTRY

www.rsc.org/materialsB

Cite this: DOI: 10.1039/c0xx00000x

www.rsc.org/xxxxxx

ARTICLE TYPE

Fabrication of chitosan/bioglass three-dimensional porous scaffold for bone tissue engineering application

Jun Yang[a,1], Teng Long[b,1], Nan-Fei He[c], Ya-Ping Guo[a*], Zhen-An Zhu[b*], Qin-Fei Ke[a*]

Received (in XXX, XXX) Xth XXXXXXXXX 20XX, Accepted Xth XXXXXXXXX 20XX
DOI: 10.1039/b000000x

Bone defects cased by trauma and disease have become urgent problems. Ideal three-dimensional (3D) porous scaffolds for bone tissue engineering application should possess interconnected porous structure, good biocompatibility and mechanical properties well-matched with natural bones. Herein, a chitosan/bioglass (CS/BG) 3D porous scaffold has been fabricated according to the following steps: (i) preparation of CS fiber 3D porous scaffold by needle-punching process and (ii) deposition of BG on the above CS fiber 3D porous scaffold by dip-coating technique. The CS/BG 3D porous scaffold has interconnected porous structure with a porosity of 77.52 % and a pore size of about 50 μm. Water absorption values of CS fiber 3D porous scaffold and CS/BG 3D porous scaffold are 570 % and 59 %, respectively. The BG in the CS/BG 3D porous scaffold significant decreases the swelling behaviour of CS fibers, and thus improves the stability of scaffolds. The CS/BG 3D porous scaffold possesses good mechanical properties with a compression strength of 7.68 ± 0.38 MPa and an elastic modulus of 0.46 ± 0.02 GPa, which are well-matched with those of trabecular bones. *In vitro* cell assay results demonstrate that the CS/BG 3D porous scaffold has good biocompatibility, which can facilitate the spreading and proliferation of human bone marrow stromal cells (hBMSCs). Therefore, the CS/BG 3D porous scaffold is a potential material for bone tissue engineering application.

1. Introduction

Bone tissue engineering has received great attentions due to its success in repair and regeneration of bone defects, but synthesis of ideal extracellular supporting materials still remains great challenges.[1-3] Among a vary of biomaterials for bone tissue engineering, chitosan (CS) is considered as a promising polymer because it has similar structure to the glycosaminoglycans of natural bones and possesses excellent biocompatibility, biodegradability and antimicrobial property. CS is a polysaccharide-type biological polymer, containing many reactive amine and hydroxyl groups that can promote osteoblast growth and enhance *in vivo* bone formation.[4-7] Moreover, CS exhibits non-antigenic, antimicrobial and antitumor properties, so it has been widely used for drug delivery, wound healing and tissue engineering.[8]

Although CS is a promising biomedical material for bone tissue engineering regeneration, it exhibits the poor mechanical properties that limit its clinical application, especially for weight-bearing bones.[9-11] To overcome the above problem, several strategies have been developed to fabricate CS-based composite scaffolds with good mechanical properties, including incorporation of another polymer such as gelatin and poly-L-lactic acid (PLA), or addition of a reinforcement bioceramic such as bioglass (BG) and hydroxyapatite (HAp).[12-14] Unlike polymer, bioceramics possess appropriate degradation that matches the formation rate of new bone, and their degradation products have no biological toxicity. Notably, BG has good biocompatibility and bioactivity, which can be integrated with surrounding bone tissue closely *in vivo* by forming a calcium phosphate layer to bond with living bone.[15-18] Moreover, it is easy to control the biodegradability of BG by changing its chemical compositions. In recent decades, a number of BG materials with different chemical compositions have been developed. The above advantages make it possible to design BG-based bone repair materials with suitable degradation rate to match that of bone ingrowth.[19-23] Previous reports have demonstrated that BG (58S, $60SiO_2$-36CaO-$4P_2O_5$) is fit for bone repair materials because of its excellent biocompatibility, bioactivity and biodegradability.[24,25] In addition, the percentages of bioceramics may greatly affect the mechanical properties of porous CS/BG scaffolds. If the percentages of bioceramics in the composite scaffold are low, no sufficient improvement in mechanical strength can be achieved. In contrast, if too many bioceramics are added in the composite scaffold, the good mechanical properties are obtained at the cost of decreasing macroporous size and porosity.[26-29]

As we now know, a 3D macroporous structure is considered to be one of the most important factors for an ideal scaffold, because macropores can promote cell ingrowth and transport of nutrients, oxygen and growth factors.[30-33] Recently, many fabrication techniques have been reported in the literatures to establish

interconnected 3D macroporous scaffolds, which include pore-forming agent technology, polymeric sponge impregnation process, foaming, sol-gel method, extrusion forming, gel-casting and thermally induced phase separation.[34,35] These methods can produce the macroporous network with a pore size of 100-600 μm and a highly porosity up to 90 %. However, their mechanical properties are too poor to match natural bones.

In order to make bone scaffolds possess macroporous structure and good mechanical properties, we fabricate a CS/BG 3D porous scaffold according to the following steps. Firstly, a 3D interconnected macroporous CS fiber 3D porous scaffold has been fabricated by needle-punching process. This method involves only physical process that has no influence on the inherent biological properties of CS.[36,37] Secondly, BG deposits on the above CS fiber 3D porous scaffold by dip-coating technique. The main aims of this work are to fabricate a CS/BG 3D porous scaffold, and to investigate its formation mechanism, phase structure, porous structure and mechanical property. In addition, the biocompatibility of the CS/BG 3D porous scaffold is investigated by using human bone marrow stromal cells (hBMSCs) as cell models.

2. Experimental

2.1 Preparation of CS fiber 3D porous scaffold

The CS fiber 3D porous scaffold was produced by needle-punching process. Briefly, chitosan staple fibers were carded to form a fibrous web by using laboratory carding machine (ASI8IA, Jiangxi textile equipment Co., Ltd, China). Eight layers of the carded fibrous webs were arranged along the machine direction, then were needled by using a needle machine (F22G-I1600, Changshu Weicheng Non-Woven Equipment Co., Ltd, China) equipped with 4500 needles (15×18×32×3 R333 G3027, Groz-Beckert, Germany) per running meter. The working frequency is 690 needles per minute and the needle rate is 3.63 m/min. The thickness and surface density of the fiber scaffold was 3.49 ± 0.26 mm and 430.08 ± 37.52 g/m^2 respectively.

2.2 Preparation of BG

BG with a molar ratio of SiO_2:CaO:P_2O_5=60:36:4 was prepared by a sol-gel method. Briefly, 2.4 g of calcium nitrate tetrahydrate, 5.53 mL of tetraethyl orthosilicate, 0.36 mL of triethyl phosphate and 58 mL of ethanol were mixed, followed by the addition of dilute nitric acid (2 mL, 1.0 mol/L) as catalytic hydrolysis. The mixture was stirred for 4 h at 40 °C, and was aged for 1 day to form a sol and another 2 days to form a gel. The BG was obtained by sintering the gel at 600 °C for 6 h with a heating rate of 3 °C/min. The BG was ground using alcohol as the medium by a planetary ball mill (Ntu Buddha electronics co., Ltd, Nanjing, China) for 12 h at a fixed speed of 360 r/min. Finally, the BG powders with a particle size of smaller than 5 μm were dried in a vacuum oven at 60 °C for 6 h.

2.3 Preparation of CS/BG 3D porous scaffold

4.0 g of ethyl cellulose (EC) was dissolved in ethanol (100 mL) at room temperature followed by addition of 20.0 g of BG powders. The mixture was stirred at 40 °C to form a BG/ethanol suspension. The CS fiber 3D porous scaffold was immersed into the above suspension, and then was withdrawn at a rate of 1 mm/s. Finally, the obtained CS/BG 3D porous scaffold was dried at 60 °C for 24 h at a humid atmosphere.

2.4 Characterization

The morphology and microstructure of samples were investigated by using field-emission scanning electron microscopy (FESEM, Hitachi S-4800, CamScan). The phases of samples were examined by X-ray power diffraction (XRD, D/max- II B, Japan). Pore structure of samples was measured by Capillary Flow Porometer (CFP, Through-pore size analyser, Porometer 3G zh, Quantachrome Instruments Ltd., Florida, USA). The porosity (P) of samples was obtained by measuring the weight of samples in dry and wet atmosphere, respectively.

$$P = (W_1\text{-}W_2)/(\rho \cdot V) \quad (1)$$

where W_1, W_2 are the wet weight and the dry weight of the material respectively, ρ is the density of the pororil wetting fluid (Quantachrome Instruments Ltd., Florida, USA) with a defined surface tension of 16 dynes/cm, and V is the total volume of the samples.

2.5 Water uptake capacity

Samples were immersed in a phosphate buffered saline (PBS, pH 7.4) at 37 °C for 30 min, 2 h, 4 h, 6 h and 8 h, respectively. When penetrated adequately, the samples were withdrawn at a rate of 1 mm/s at intervals. Water uptake value (E) was calculated according to the following equation:

$$E = (W_e\text{-}W_d)/W_d \quad (2)$$

where W_e and W_d are the wet weight and the dry weight of the samples, respectively.

2.6 Mechanical property

Mechanical properties of the samples including compression properties, flexure properties and tensile properties were analysed with different test instruments. Compression property was measured by universal material testing machine 2T (WDW3020, Changchun New Test Instrument co., Ltd., China) with a compression speed of 0.5 mm/min and the specimen size of 25 mm long, 25 mm width, and 10 mm thick. Flexure property was measured by microcomputer control electronic universal testing machine (WDW-20, Shanghai Hualong Microelectronics co., Ltd., China) with a chuck traveling speed of 1 mm/min and the specimen size of 50 mm long, 20 mm width, and 3 mm thick. Tensile property was measured by an electrical universal material testing machine (YG028-500, Changzhou First Textile Machinery co., Ltd., China) with stretching velocity of 10 mm/min and a gauge length of 40 mm. The size of the samples was 50 mm long, 20 mm width, and 3 mm thick. Each measurement was performed three times. Besides, the fracture toughness of the samples was measured by the single edge notched beam (SENB) technique.[38] Fracture toughness (K) was calculated according to the equation:

$$K = \frac{3PL}{2BW^2}\sqrt{a} \cdot y \quad (3)$$

where P is the applied loading, L is the three-point bending span, B is the width of the sample, W is the thickness of the sample, a is

the depth of the notch, and *y* is the dimensionless parameter.

2.7 Cell behaviours

2.7.1 Cell culture

Human bone marrow stromal cells (hBMSCs) were obtained and expanded according to the literature.[39] The study was approved by the Ethics Committee of the Ninth People's Hospital of Shanghai Jiao Tong University. Cells were cultured in α-modified minimum essential medium (α-MEM), supplemented with 10 % fetal bovine serum (FBS), 1 % penicillin (100 U/mL), and streptomycin sulphate (100 mg/mL, Gibco, Grand Island, NY). The medium was changed every 2 days.

2.7.2 Cell proliferation assay

The proliferation assay was performed by using the cell counting kit-8 (CCK-8, Dojindo, Kumamoto, Japan) according to the manufacturer's instructions. Briefly, samples with a diameter of 15 mm and a thickness of 3 mm were seeded at 2×10^4 cells per sample in a 24-well plate. At each time-point, 100 μL of water-soluble tetrazolium-8 solution was added to each well, and plates were incubated for 2 h at 37 °C. 200 μL solution of each well was added into a new 96-well plate, and the corresponding absorbance was measured at 450 nm by a micro plate spectrophotometer (Bio-Rad Laboratories, Hercules, CA).

2.7.3 Cell morphology

Cell morphologies on CS fiber 3D porous scaffold and CS/BG 3D porous scaffold were investigated by fluorescence staining. Briefly, after culturing hBMSCs at 2×10^4 cells per sample for 24 h, samples were gently washed with PBS and maintained in 4% paraformaldehyde for 15 min, followed by immersing in 0.1% Triton X-100 solution for 15 min. TRITC phalloidin was used to stain the actin filaments of cells as red fluorescent light, and 4', 6-diamidino-2-phenylindole (DAPI) was used to stain the nucleus of cells as blue fluorescent light. The cytoskeleton of hBMSCs was observed under laser scanning confocal microscopy (LSCM, LEICA TCS SP2, Heidelberg, Germany).

2.8 Statistical analysis

Results are presented as means ± SD. Statistical analysis are conducted by analysis of variance (ANOVA). All experiments were performed in triplicate. (*) denotes significant difference with $P < 0.05$, and (**) denotes significant difference with $P < 0.01$.

3. Results

3.1 Morphology, porous structure and phase of CS/BG 3D porous scaffold

The FESEM images of CS fiber 3D porous scaffold and CS/BG 3D porous scaffold are shown in Fig. 1. The CS fiber 3D porous scaffold produced by needle-punching process has a smooth surface and uniform diameter of about 15 μm (Fig. 1a and b). After the dip-coating process, a layer of BG powders deposits on the CS fiber 3D porous scaffold. The CS/BG 3D porous scaffold has a rough surface and uniform diameter of about 18 μm. The BG powders exist as irregular shape with particle size of 1~5 μm. Fig. 1 shows that both the CS fiber 3D porous scaffold and CS/BG 3D porous scaffold possess interconnected macroporous structure, as confirmed by the pore size distribution curves (Fig. 2). The graphs show the percentage of the current pore number over the total pore number (black line) and the percentage of the cumulative number from current pore size to the maximum pore size over the total pore number (blue line). The pore size of the CS fiber 3D porous scaffold is mainly distributed at around 60 μm, while that of the CS/BG 3D porous scaffold is mainly distributed at around 50 μm (Fig. 2). Moreover, Table 1 shows that the porosities of the CS fiber 3D porous scaffold and CS/BG 3D porous scaffold are 86.78 % and 77.52 %, respectively. The smaller pore size and porosity of the CS/BG 3D porous scaffold than the CS fiber 3D porous scaffold are attributed to the presence of BG particles in the composite scaffold.

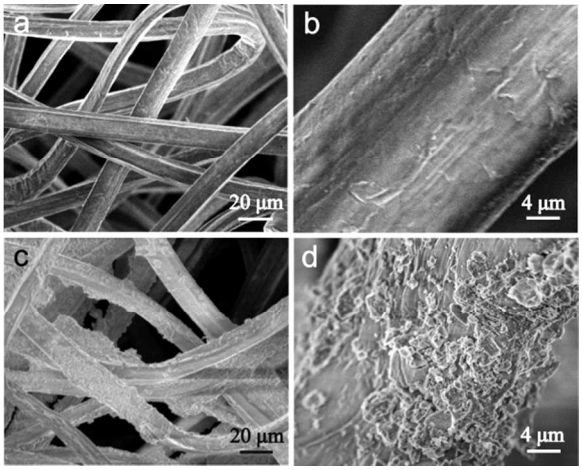

Fig. 1 FESEM images of samples: (a, b) CS fiber 3D porous scaffold; (c, d) CS/BG 3D porous scaffold.

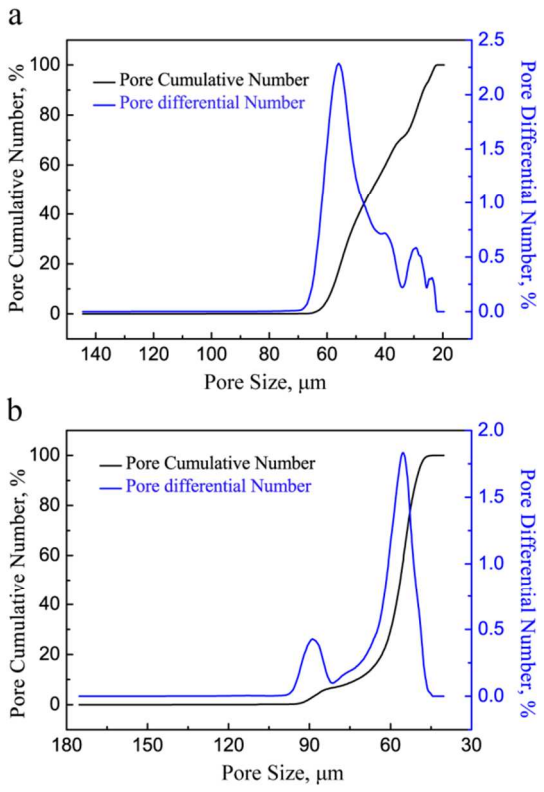

Fig. 2 Pore size distribution curves of samples: (a) CS fiber 3D porous scaffold; (b) CS/BG 3D porous scaffold

Table 1 Porosity and water uptake value of CS fiber 3D porous scaffold and CS/BG 3D porous scaffold

Samples	Porosity (%)	Water absorption (%)
CS fiber 3D porous scaffold	86.78 ± 1.65	569.52 ± 61.76
CS/BG 3D porous scaffold	77.52 ± 1.67	58.89 ± 7.32

The water uptake capacities of the CS fiber 3D porous scaffold and CS/BG 3D porous scaffold are measured, as shown in Table 1. The water uptake value of CS fiber 3D porous scaffold is about 570 % owing to the swelling behaviour of CS fiber 3D porous scaffold. After the addition of BG powders, the water uptake value of the CS/BG 3D porous scaffold reduces to about 59 %.

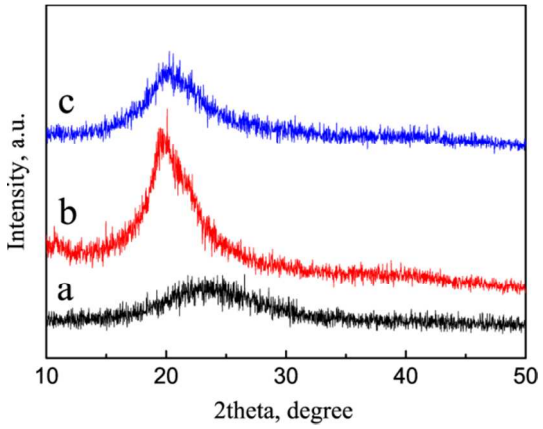

Fig. 3 XRD patterns of samples: (a) BG powders; (b) CS fiber 3D porous scaffold; (c) CS/BG 3D porous scaffold.

The XRD patterns of BG powders, CS fiber 3D porous scaffold and CS/BG 3D porous scaffold are shown in Fig. 3. A wide diffraction peak between 18° and 30° is observed for BG powders (Fig. 3a), which belongs to the characteristic peak of amorphous materials. CS, a random copolymer of N-acetyl-D-glucosamine and D-glucosamine, is the partially de-acetylated derivative of chitin. The CS fiber 3D porous scaffold exhibits a broad peak at around 2θ=20.6° because it is a semi-crystalline material (Fig. 3b).[40] Fig. 3c indicates that the CS/BG 3D porous scaffold possesses the characteristic peaks of both CS and amorphous BG.

3.2 Mechanical property of CS/BG 3D porous scaffold

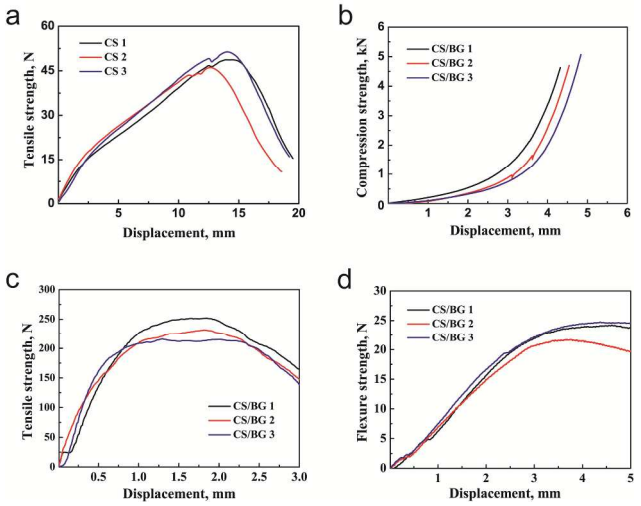

Fig. 4 (a) Mechanical response in tensile for CS fiber 3D porous scaffold. CS 1, 2, 3 are fabricated under the same conditions. Mechanical response for CS/BG 3D porous scaffold: (b) compression, (c) tensile and (d) flexure. CS/BG 1, 2, 3 are fabricated under the same conditions.

The relation curves of mechanical strength and displacement for the scaffolds, including compression strength, flexure strength and tensile strength, are shown in Fig. 4. The mechanical parameters of the CS fiber 3D porous scaffold and CS/BG 3D porous scaffold are summarized in Table 2. The samples tested in this study are fabricated under the same conditions. The CS fiber 3D porous scaffold as a kind of soft ductile material has good tensile property, but exhibits poor compression property and flexure property. When compressed by external force, this scaffold undergoes only compression deformation without brittle fracture process. Therefore, the CS fiber 3D porous scaffold has no compression property or flexure property. In contrast, the CS/BG 3D porous scaffold exhibits good compression strength of 7.68 ± 0.38 MPa and elastic modulus of 0.46 ± 0.02 GPa, which are in agreement with the compression performance of trabecular bone exactly.[41,42] Although BG is a brittle material, the CS/BG 3D porous scaffold has good tensile and flexure properties because the CS fibers in the composite scaffold act as reinforcing materials.

Table 2 Mechanical properties of CS/BG 3D porous scaffold in compression, tensile and flexure

Samples	Compression Strength (MPa)	Elastic modulus (GPa)	Flexure Strength (MPa)	Flexure modulus (MPa)	Tensile Strength (MPa)	Tensile Modulus (MPa)	Fracture toughness (MPa·m$^{1/2}$)
CS fiber 3D porous scaffold					0.68 ± 0.06	3.40 ± 0.24	
CS/BG 3D porous scaffold	7.68 ± 0.38	0.46 ± 0.02	6.0 ± 0.4	102.0 ± 10.0	3.11 ± 0.24	196.0 ± 17.0	0.24 ± 0.02
Trabecular bone [42]	4 - 12	0.1 - 0.5					0.1-0.8

3.3 Biocompatibility of CS/BG 3D porous scaffold

An ideal bone scaffold should be biocompatible with surrounding cells to promote satisfactory osteointegration between the scaffold and bone tissue. Here, the biocompatibility of the CS/BG 3D porous scaffold on the cell spreading and proliferation are evaluated by using hBMSCs as a cell model. As we know, CCK-8 assay is a quick and effective method for testing mitochondrial impairment and correlates quite well with cell proliferation. Fig. 5 shows the CCK-8 results of the hBMSCs cultured on the CS fiber 3D porous scaffold and CS/BG 3D porous scaffold at different days. Upon increasing the culture time, the number of viable cells on both the CS fiber 3D porous scaffold and CS/BG 3D porous scaffold continues to increase. As compared with the CS fiber 3D porous scaffold, the more viable cells are observed on the CS/BG 3D porous scaffold at each time-point, suggesting that the CS/BG 3D porous scaffold has better biocompatibility to promote the adhesion and proliferation of hBMSCs.

Fig. 6 shows the LSCM images of the hBMSCs cultured on the CS fiber 3D porous scaffold and CS/BG 3D porous scaffold for 24 h. An actin cytoskeleton and focal adhesion staining kit is used to map the orientation of actin filaments with TRITC phalloidin and to label nuclei with DAPI. The long red bundles of stress fibers composed of actin filaments and good cell-cell contact with one another demonstrate the good cell cytoskeleton morphology

of the hBMSCs on both the CS fiber 3D porous scaffold and CS/BG 3D porous scaffold. The hBMSCs on the CS fiber 3D porous scaffold exhibit a fusiform-shaped and stereo morphology. Notably, as compared with the CS fiber 3D porous scaffold, the hBMSCs cultured on the CS/BG 3D porous scaffold exhibit rearranged cytoskeleton with better-developed stress actin fibers and stronger actin intensity (Fig. 6), suggesting that the CS/BG 3D porous scaffold possesses more excellent cell adhesion and spreading.

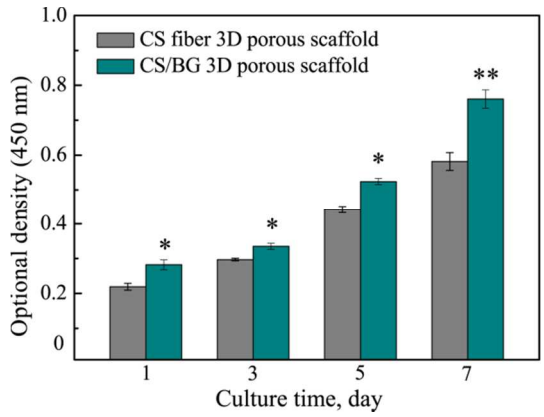

Fig. 5 CCK-8 assay results of hBMSCs cultured on CS fiber 3D porous scaffold and CS/BG 3D porous scaffold at different days.

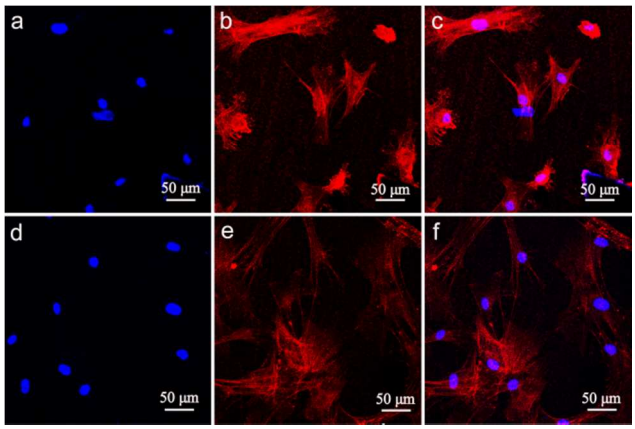

Fig. 6 LSCM images of cytoskeletal morphology of hBMSCs after culturing for 24 h on the different samples: (a, b, c) CS fiber 3D porous scaffold, and (d, e, f) CS/BG 3D porous scaffold. The actin filaments were stained as red fluorescent light and the nucleus were stained as blue fluorescent light.

4. Discussion

Recently, CS has been widely used for bone tissue engineering because of its excellent biocompatibility, biodegradability, and antimicrobial property. However, pure CS scaffold exhibits poor mechanical properties, which limit its clinic applications for weight-bearing bones.[4,11] In this work, we have successfully fabricated a CS fibers-based scaffold with improved mechanical strength by addition of BG powders as reinforcement agent. The incorporation of BG into the CS fiber 3D porous scaffold significantly improves the biocompatibility of the composite scaffold (CS/BG 3D porous scaffold) to support cell adhesion, proliferation and spreading. Besides the chemical components, the porous structure and porosity affect greatly the biocompatibility of bone scaffold. The desired bone scaffold should have macroporous network with high porosity and interconnected pore system, similar to the morphology of extracellular matrix (ECM). The interconnected pores with a high porosity not only promote cell adhesion, proliferation and growth, but also allow the transport of nutrient, oxygen, and the removal of metabolic products.[43,44] Herein, we fabricate the CS/BG 3D porous scaffold according to the following steps (Fig. 7). Firstly, the CS fiber 3D porous scaffold is prepared by needle-punching process (Fig. 7a and b). The CS fiber 3D porous scaffold exhibits the 3D macroporous structure with a pore size of about 60 μm and a porosity of about 86.78 % (Fig. 1a and Table 1). Secondly, the CS/BG 3D porous scaffold is produced by deposition of a layer of BG powders on the surface of CS fiber 3D porous scaffold via a dip-coating technique (Fig. 7d-f). The CS/BG 3D porous scaffold possesses also macroporous structure with a pore size of 50 μm, which is smaller than that of CS fiber 3D porous scaffold (Fig. 2). Moreover, the porosity of the CS/BG 3D porous scaffold is lower than that of the CS fiber 3D porous scaffold because the BG powders are incorporated in the composite scaffold (Table 1 and Fig. 1).

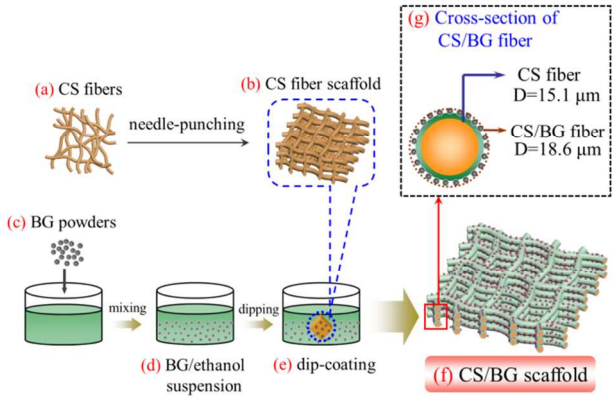

Fig. 7 Illustration of the fabrication strategy of CS/BG 3D porous scaffold: (a) CS fibers used as original materials; (b) preparation of CS fiber 3D porous scaffold by needle-punching process; (c) BG powders; (d) formation of BG/ethanol suspension by addition of BG powders into ethanol; (e) preparation of CS/BG 3D porous scaffold by dip-coating method; (f) CS/BG 3D porous scaffold; (g) cross-sectional view of CS/BG fiber.

Swelling behaviour and structure stability of the scaffolds are critical for their particular applications in bone tissue engineering. Most natural polymers such as CS are easily swelled in biological fluids. Initial swelling is essential for the porous CS fiber scaffold, and the possible resultant increase of its pore size can facilitate cell adhesion, proliferation and growth. However, continuous swelling may decrease the mechanical strength and affect the stability so that the scaffold is failed to provide the basic support for new tissue formation. Therefore, the swelling ability of scaffold materials should be controlled within a specific range.[45-47] The swelling behaviour of the scaffold can be represented with its water uptake capacity. As is shown in Table 1, the water uptake value of the CS fiber 3D porous scaffold is up to nearly 570 % because the long chain structure of CS and the small molecular of solvent promote the diffusion of the solvent molecules into the polymer. The water uptake value of the CS/BG 3D porous scaffold falls down to about 59 % on account of the layer of BG powders that retain the structure integrity of

the scaffold.

For bone tissue engineering scaffold, its tailored mechanical strength similar to natural bone provides a substitute initially for wound contraction forces and later for the remodelling of bone tissue. The mechanical properties of the scaffold mainly depend on the architectural characteristics including the pore structure, porosity and pore size. High porosity and large pore size favour cell adhesion, proliferation and formation of new bone tissue, but lead to poor mechanical properties. To overcome this problem, we need to find a balance between the biological performance and mechanical properties in designing an ideal scaffold.[48,49] For a single material, CS fiber 3D porous scaffold has various advantageous biological properties, but the poor mechanical properties hinder its application in hard-tissue scaffolds. To improve the mechanical properties, needle-punching process is proposed particularly to construct a porous CS fiber 3D porous scaffold with good tensile properties (Fig. 4a). As compared with electrospinning technology, needle-punching method possesses its unique advantages to build a 3D macroporous scaffold with a uniform pore size distribution. The whole process involves only a physical change, and has no obvious influence on the inherent biological properties of CS.

The CS fiber 3D porous scaffold is a kind of non-brittle material with poor compression properties. When compressed by external force, the scaffold channel produces uncertain damage and the 3D porous structure is destroyed. For an ideal scaffold composed of non-brittle materials, its compression process exhibits elastic bending deformation at small strain, then plastic yielding deformation at large strain, followed by brittle fracture process at much large strain.[50] However, CS fiber 3D porous scaffold is a totally soft ductile material that undergoes only compression deformation, without brittle fracture process. To improve its compression properties, a layer of BG powders deposits on the surface of the CS fiber 3D porous scaffold, revealing a tough-brittle transition. Table 1 shows that the compression strength and elastic modulus of the CS/BG 3D porous scaffold match well with those of trabecular bone.[41,42] The better mechanical properties of CS/BG 3D porous scaffold are mainly attributed to the addition of BG powders on the surface of CS fiber 3D porous scaffold. BG is a typical brittle material that can increase the hardness of each CS fiber. On the other hand, the increase in the diameter of CS fiber may give more paths for distributing the applied stress and function as a barrier against crack propagation.

Excellent biocompatibility is one of the most important factors for bone engineering tissue application. An ideal scaffold should provide a suitable microenvironment to support the appropriate cellular activity, including cell attachment, spreading, proliferation and lineage differentiation. Notably, there are many factors that may influence the biocompatibility of bone scaffolds including pore size distribution, composition and mechanical properties.[51] Since hBMSCs are marrow-derived cell and play a vital role in the process of bone regeneration, they serve as cell models to investigate the biocompatibility of the CS fiber 3D porous scaffold and CS/BG 3D porous scaffold. CCK-8 assay results show that the number of viable cells on both the CS fiber 3D porous scaffold and CS/BG 3D porous scaffold increases in a time dependent manner, suggesting their good biocompatibility. More viable cells are observed on the CS/BG 3D porous scaffold than on the CS fiber 3D porous scaffold at each time-point (Fig. 5). The above results indicate that the CS/BG 3D porous scaffold possesses better biocompatibility to promote the adhesion and proliferation of hBMSCs than the CS fiber 3D porous scaffold. To further verify the biocompatibility of the scaffold, the actin cytoskeleton and focal adhesion staining kit has been used to examine the morphology of hBMSCs on the CS fiber 3D porous scaffold and CS/BG 3D porous scaffold. The hBMSCs on the CS fiber 3D porous scaffold and CS/BG 3D porous scaffold exhibit a fusiform-shaped and stereo morphology spreading along the direction of the fiber channel. Interestingly, cells are more viably distributed and display better cell-spreading spread cytoskeleton morphology on the CS/BG 3D porous scaffold than on the CS fiber porous scaffold (Fig. 6). The excellent biocompatibility of the CS/BG 3D porous scaffold may be attributed to its pore size distribution, chemical composition and mechanical property. Firstly, a large pore size is benefit for cell adhesion, proliferation and growth. Fig. 2a reveals that the pore size of CS fiber 3D porous scaffold is mainly distributed at about 60 μm. Secondly, BG is an accepted bone repair materials with good biocompatibility and bioactivity. By achieving sound integration with surrounding bone tissue *in vivo* through forming a calcium phosphate layer on the surface, BG can efficiently promote bone repair. The presence of BG powders significantly improves the biocompatibility of the CS/BG 3D porous scaffold to support cell adhesion, proliferation and spreading *in vitro*.[52,53] Finally, the mechanical properties of CS/BG 3D porous scaffold are similar to trabecular bone. As is well known, tissue-level matrix stiffness exerts very strong effects on the focal-adhesion structure, the cytoskeleton system and lineage specification of hBMSCs. The CS/BG 3D porous scaffold mimics collagenous trabecular bone in the mechanical properties, which not only promotes the cell attachment and proliferation, but also induces the osteogenic differentiation of hBMSCs.[54]

5. Conclusion

A CS/BG 3D porous scaffold including CS fibers and BG powders is fabricated according to the following steps: (i) preparation of CS fiber 3D porous scaffold by needle-punching process and (ii) deposition of BG on the above CS fiber 3D porous scaffold by dip-coating technique. The CS/BG 3D porous scaffold has the interconnected macroporous structure with high porosity to supply enough space for cell ingrowth and transport of nutrients. The lower water uptake capacity of the CS/BG 3D porous scaffold than the CS fiber 3D porous scaffold significantly alleviates the swelling behaviour of CS and improves the stability of scaffold structure. The mechanical properties of CS/BG 3D porous scaffold are well-matched with trabecular bone. *In vitro* assay results demonstrate that the CS/BG 3D porous scaffold has good biocompatibility to facilitate the attachment, spreading and proliferation of hBMSCs. Therefore, the CS/BG 3D porous scaffold has great potential for the repair of bone defects.

Acknowledgements

This research was supported by Key Disciplines of Shanghai Municipal Education Commission (No. J50206), Natural Science

Foundation of China (Nos. 51002095 and 51372152), Science and Technology Commission of Shanghai Municipality (No. 12JC1405600), Program of Shanghai Normal University (Nos. DZL124 and DCL201303), Innovation Foundation of Shanghai Education Committee (No. 14ZZ124), and State Key Laboratory for Modification of Chemical Fibers and Polymer Materials, Donghua University (No. LK1206).

Notes and references

[1] J. Yang and T. Long contributed equally to this work.

[a] *The Education Ministry Key Lab of Resource Chemistry and Shanghai Key Laboratory of Rare Earth Functional Materials, Shanghai Normal University, Shanghai 200234, P. R. China. Fax: +86-21-64321951; Tel: +86-21-64321951; E-mail: kqf@shnu.edu.cn (Q. F. Ke); ypguo@shnu.edu.cn (Y. P. Guo)*

[b] *Shanghai Key Laboratory of Orthopedic Implant, Department of Orthopedic Surgery, Shanghai Ninth People's Hospital, Shanghai Jiao Tong University School of Medicine, Shanghai 200011, China. E-mail: zhuzhenan2006@126.com (Z. A. Zhu)*

[c] *State Key Laboratory for Modification of Chemical Fibers and Polymer Materials, College of Textiles, Donghua University, Shanghai 200234, P. R. China.*

1 F. J. OBrien, Mater. *today*, 2011, **14**, 88-95.
2 A. J. Salinas, P. Esbrit and M. Vallet-Regi, *Biomater. Sci.*, 2013, **1**, 1-100.
3 S. Bose, M. Poy and A. Bandyopadhyay, *Trends Biotechnol.*, 2012, **30**, 546-554.
4 S. K. Lan Levengood and M. Q. Zhang, *J. Mater. Chem. B*, 2014, **2**, 3161-3184.
5 F. Croisier and C. Jerome, *Eur. Polym. J.*, 2013, **49**, 780-792.
6 S. K. Nandi, B. Kundu and D. Basu, *Mater. Sci. Eng. C*, 2013, **33**, 1267-1275.
7 P. Ghosh, A. Prabhu R., N. Dogra and S. Dhara, *RSC Adv.*, 2014, **4**, 19516-19524.
8 R. Jayakumar, M. Prabaharan, P.T. Sudheesh Kumar, S.V. Nair and H. Tamura, *Biotechnol. Adv.*, 2011, **29**, 322-337.
9 M. Z. Albanna, T. H. Bou-Akl, O. Blowytsky, H. L. Walters, H. W. Matthew, *J. Mech. Behav. Biomed.*, 2013, **20**, 217-226.
11 K. Lee, G. Jin, C. H. Jang, W. K. Jung and G. H. Kim, *J. Mater. Chem. B*, 2013, **1**, 5831-5841.
12 F. Pishbin, A. Simchi, M.P. Ryan and A.R. Boccaccini, *Surf. Coat. Tech.*, 2013, **20**, 173-183.
13 D. M. Luo, L. Sang, X. L. Wang, S. M. Xu and X. D. Li, *Mater. Lett.*, 2011, **65**, 2395-2397.
14 Q. Q. Yao, P. Nooeaid, J. A. Roether, Y. M. Dong, Q. Q. Zhang and A. R. Boccaccini, *Ceram. Int.*, 2013, **39**, 7517-7522.
15 A. J. Salinas and M. Vallet-Regi, RSC Adv., 2013, 3, 11116-11131.
16 J. Hum and A. R. Boccaccini, *J. Mater. Sci. Mater. Med.*, 2012, **23**, 2317-2333.
17 J. R. Jones, *Acta Biomater.*, 2013, **9**, 4457-4486.
18 W. Holand, W. Vogel, K. Naumann and J. Gummel, *J. Biomed. Mater. Res. A*, 1985, **19**, 303-312.
19 Q. Fu, E. Saiz, M. N. Rahaman and A. P. Tomsia, *Mater. Sci. Eng. C*, 2011, **31**, 1245-1256.
20 A. Hoppe, V. Mourino and A. R. Boccaccini, *Biomater. Sci.*, 2013, **1**, 254-256.
21 E. A. Abou Neel, D. M. Pickup, S. P. Valappil, R. J. Newport and J. C. Knowles, *J. Mater. Chem.*, 2009, **19**, 690-701.
22 M. N. Rahaman, D. E. Day, B. S. Bal, Q. Fu, S. B. Jung, L. F. Bonewald and A. P. Tomsi, *Acta Biomater.*, 2011, **7**, 2355-2373.
23 G. Kaur, O. P. Pandey, K. Singh, D. Homa, B. Scott and G. Pickrell, *J. Biomed. Mater. Res. A*, 2014, **102**, 254-274.
24 R. C. Bielby, R. S. Pryce, L. L. Hench and J. M. Polak, *Tissue Eng.*, 2005, **11**, 479-488.
25 H. Y. Li, R. L. Du and J. Chang, *J. Biomater. Appl.*, 2005, **20**, 137-155.
26 R. Pallela, J. Venkatesan, V. R. Janapala and S. K. Kim, *J. Biomed. Mater. Res. A*, 2012, **100**, 486-495.
27 M. X. Liu, C. C. Wu, Y. P. Jiao, S. Xiong and C. R. Zhou, *J. Mater. Chem. B*, 2013, **1**, 2078-2089.
28 H. L. Fan, L. L. Wang, K. K. Zhao, N. Li, Z. J. Shi, Z. G. Ge and Z. X. Jin, *Biomacromolecules*, 2010, **11**, 2345-2351.
29 J. Venkatesan and S. K. Kim, *Mar. Drugs*, 2010, **8**, 2252-2266.
30 F. Baino and C. Vitale-Brovarone, *J. Biomed. Mater. Res. A*, 2011, **97**, 514-535.
31 S. Eshraghi and S. Das, *Acta Biomater.*, 2010, **6**, 2467-2476.
32 C. M. Walthers, A. K. Nazemi, S. L. Patel, B. M. Wu and J. C. Y. Dunn, *Biomaterials*, 2014, **35**, 5129-5137.
33 A. Shekaran and A. J. Gracia, *J. Biomed. Mater. Res. A*, 2011, **96**, 261-272.
34 B. Stevens, Y. Z. Yang, A. Mohandas, B. Stucker and K. T. Nguyen, *J. Biomed. Mater. Res. B*, 2008, **85**, 573-582.
35 K. K. Mallick and J. Winnett, *J. Am. Ceram. Soc.*, 2012, **95**, 2680-2686.
36 I. Rajzer, J. G. Pietras and J. Janicki, *Fibres. Text. East. Eur.*, 2011, **19**, 66-72.
37 Y. J. Yeo, D. W. Jeon, C. S. Kim, S. H. Choi, K. S. Cho, Y. K. Lee and C. K. Kim, *J. Biomed. Mater. Res. B*, 2005, **72**, 86-93.
38 R. Damani, R. Gstrein and R. Danzer, *J. Eur. Ceram. Soc.*, 1996, 16, 695-702.
39 H. L. Sun, C. T. Wu, K. R. Dai, J. Chang and T. T. Tang, *Biomaterials*, 2006, **27**, 5651-5657.
40 M. Peter, N. S. Binulal, S. Soumya, S. V. Nair, T. Furuike, H. Tamura and R. Jayakumar, *Carbohyd. Polym.*, 2010, **79**, 284-289.
41 A. J. Wagoner Johnson and B. A. Herschler, *Acta Biomater.*, 2011, **7**, 16-30.
42 K. Rezwan, Q. Z. Chen, J. J. Blaker and A. R. Boccaccini, *Biomaterials*, 2006, **27**, 3413-3431.
43 S. P. Huang, Z. Chen, N. Pugno, Q. Chen and W. F. Wang, Mater. Lett., 2014, **122**, 315-319.
44 R. A. Marklein, D. E. Soranno and J. A. Burdick, *Soft Matter*, 2012, **8**, 8113-8120.
45 Y. Q. Yu, F. Q. Jia, S. H. Li, S. P. Yan, C. F. Leng and K. S. Yuan, *Int. J. Polym. Mater.*, 2013, **62**, 450-454.
46 K. Huanbutta, K. Cheewatanakornkool, K. Terada, J. Nunthanid and P. Sriamornsak, *Carbohyd. Polym.*, 2013, **97**, 26-33.
47 Q. B. Wei, Y. L. Luo, F. Fu, Y. Q. Zhang and R. X. Ma, *J. Appl. Polym. Sci.*, 2013, **129**, 806-814.
48 S. Nardecchia, D. Carriazo, M. L. Ferrer, M. C. Gutierrez and F. Monte, *Chem. Soc. Rev.*, 2013, **42**, 794-830.
49 J. J. Kim, R. K. Singh, S. J. Seo, T. H. Kim, J. H. Kim, E. J. Lee and H. W. Kim, *RSC Adv.*, 2014, **4**, 17325-17336.
50 Y. Ke, Y. J. Wang, L. Ren, Q. C. Zhao and W. Huang, *Acta Biomater.*, 2010, **6**, 1329-1336.
51 G. Thrivikraman, G. Madras and B. Basu, *RSC Adv.*, 2014, **4**, 12763-12781.
52 C. X. Xu, P. Q. Su, X. F. Chen, Y. C. Meng, W. H. Yu, A. P. Xiang and Y. J. Wang, *Biomaterials*, 2011, **32**, 1051-1058.
53 B. Marelli, C. E. Ghezzi, D. Mohn, W. J. Stark, J. E. Barralet, A. R. Boccaccini and S. N. Nazhat, *Biomaterials*, 2011, **32**, 8915-8926.
54 A. J. Engler, S. Sen, H. L. Sweeney and D. E. Discher, *Cell*, 2006, **126**, 677-689.